Smart Transformer-based single phase-to-neutral fault management

Giovanni De Carne
Marius Langwasser
Rongwu Zhu
Marco Liserre

Suggested Citation

Smart Transformer-based single phase-to-neutral fault management

Giovanni De Carne, *Member, IEEE,* Marius Langwasser, *Student Member, IEEE,* Rongwu Zhu, *Member, IEEE,*
Marco Liserre, *Fellow, IEEE,*

Abstract—The Smart Transformer, with its high control capability, offers new features for optimizing the management of the distribution grid. The ST, controlling the voltage in each phase independently, is able to manage the operations during grid faults, and in particular in the single-phase ones. The ST, when a single-phase to ground fault occurs, can rapidly reduce the voltage in the phase under fault. Thus, it guarantees system safety and operates with the remaining two healthy phases to avoid unnecessary interruption in the healthy lines. However, the two-phase asymmetrical operation challenges the system performances due to the high power 2nd harmonic ripple in the DC voltage, that reduces the capacitors lifespan, and the high current flowing in the neutral conductor. These issues would force the grid operator to increase the ST maintenance, in order to avoid unplanned faults in the ST hardware, due to failure of aged capacitors. This paper presents a flexible control strategy, based on the phase-shift angle control between two healthy-phase voltages, that reduces the impact of the power 2nd harmonic oscillation and thus can delay the maintenance intervention. The proposed strategy aims to improve system performances by avoiding neutral-line current overload and attenuating AC side active power (low voltage DC-link voltage) oscillation. Depending on the grid conditions (small DC link capacitance or low ampacity of neutral cable), the voltage angle can be adapted, minimizing the impact of the two-phase operation system in the ST-fed grid. The effectiveness and feasibility of the proposed approach have been validated experimentally with a simplified microgrid setup.

I. Introduction

IN electric power grids, the continuity of the service is a basic requirement to ensure safe operative conditions for critical loads [1]. However, it is affected by grid faults that force the disconnection of any faulty 3-phase feeder from the main grid. The impact of a fault on a LV grid varies depending on the grid short circuit power: this differs from the line impedance, the grid typology (urban, suburban or rural grid), and the load installed [2].

The Smart Transformer (ST) [3], a power electronics-based transformer that substitutes the conventional transformer (CT) in the MV/LV substation, is able to control the LV grid and shape the load consumption to offer ancillary services to the distribution grid [4]. The ST has already passed the design stage and 6 demonstrators are planned to take place

in the Scottish distribution grid, as described in the OFGEM-funded LV-ENGINE project [5], to demonstrate the achievable higher system controllability. Applying a controlled voltage or frequency variation (within the range allowed by grid rules), the ST can estimate in real time the load power sensitivity [6]. It can use this information for applying accurate power control actions, such as soft load reduction [4], the ST is able to reduce instantaneously the load power consumption, offering an alternative to classical load shedding. In case of Single Phase-to-Neutral Fault (SPNF), the ST clears the fault rapidly, blocking its semiconductor in the faulty phase. As advantage with respect to the CT, the ST can still operate with two remaining phases. Instead of disconnecting all the three phases and clearing the fault, or supplying the load with uncontrolled voltage unbalance, the ST continues to supply the connected loads. This possibility goes along with the request of having a self-healing smart grid, that, in case of fault, can support the system restoration and at the same time preserve the system integrity in the two remaining phases [7]. However, during the two-phase operations, a 2nd harmonic power oscillation is generated by the unbalance load power provision among the phases. In the case of CT, high current unbalance increases the transformer temperature, accelerating its aging [8]. In the ST case, the power oscillation causes DC-link voltage 2nd harmonic ripple, that can surpass the manufacturers suggested limit (i.e., 5% of nominal voltage [9]), which is set to preserve the lifetime of DC-link capacitors.
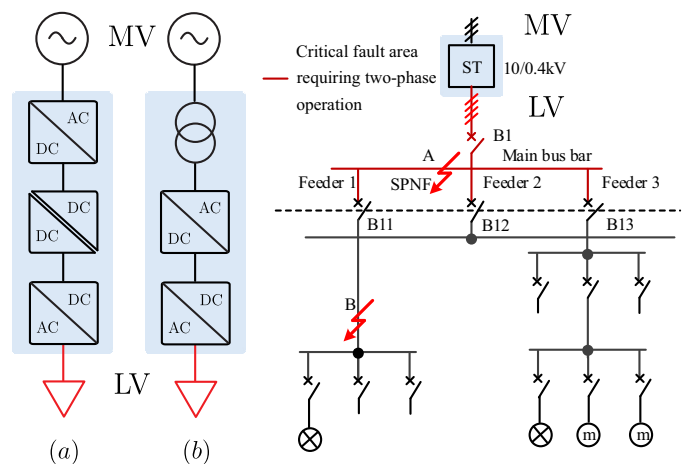
Moreover, due to the imbalance among the phases, the

Fig. 1. Bi-phase grid operation concept in case of (*a*) three-stage ST, (*b*) two-stage ST.
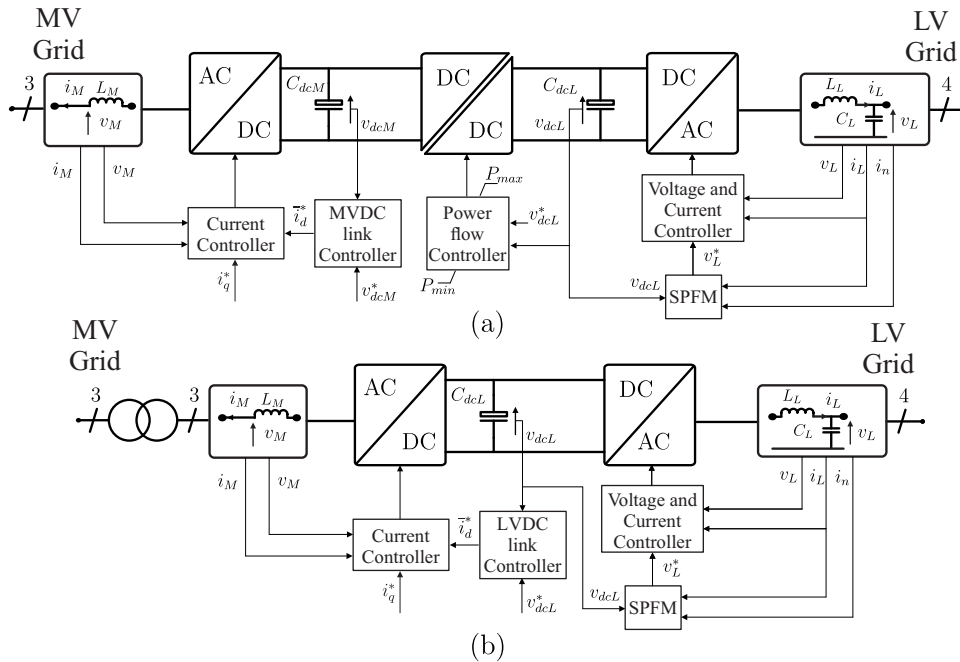
Fig. 2. ST control scheme with the indication where the Single Phase Fault Management (SPFM) act in case of (a) Three-stage ST, (b) Two-stage ST.

current flowing in the neutral conductor can reach values comparable to the phase current [10], and, in extreme cases, it can exceed the cable ampacity. Furthermore, the high neutral current makes the neutral voltage oscillating and increases the grid power losses [11], [12]. These reasons force the operator to increase the maintenance for the ST, in order to avoid unplanned hardware outage, due to the failure of aged DC capacitors, increasing the maintenance costs, as shown in [13].

In this paper, a Single-Phase Fault Management strategy is proposed. The goal of the proposed strategy is to postpone the intervention time for maintenance, limiting the impact of the 2nd harmonic power oscillation and of the neutral line current. Compared to the CT, whose phase-shift among phases is fixed at $120°$, the ST can actively control the phase-shift between the two remaining healthy phases from the initial $120°$ to any value between $0°$ and $360°$. If a SPNF occurs near the substation at the main bus bar (point A in Fig. 1), the phase-shift controller allows two-phase operation, shifting the healthy phases' angles. However, if the fault occurs in a lower branch of the grid (Point B in Fig. 1), the ST can continue the three-phase operation, keeping the angles to the nominal value, due to the minor impact of the load disconnection. Therefore, the flexible phase-shift control offers possibilities to optimize system performances, avoiding large neutral line current and consequent neutral conductor overload, while attenuating active power oscillations and preserving the DC-link capacitor. This work is structured as follows: Section II describes the ST operations during single-phase to neutral faults; in Section III the simulation of the Single Phase Fault Management (SPFM) controller are shown, aiming to minimize DC-link voltage ripple, while Section IV discusses of the impact of the SPFM controller on the connected loads. Following, an optimal tuning of the function weights is proposed in Section

V. The experimental validation of the SPFM controller with a simplified microgrid setup is carried out in Section VI, while Section VII is dedicated to conclusions.

II. ST-FED DISTRIBUTION GRID PERFORMANCES DURING SPFM

A. ST-fed distribution grid

The ST as shown in Fig. 2 can be composed of three or two stages. In the three-stage configuration, a MV AC/DC converter manages the power in order to control the voltage in the MV DC-link; the DC/DC stage adapts the voltage from the MV DC-link to the LV DC-link and regulates the power flow between the two distribution grids; and the DC/AC converter controls the voltage in the ST-fed grid. In the two stage configuration a conventional transformer steps-down the medium voltage to low voltage and the ST is operated as LV back-to-back converter, where the AC/DC-converter manages the power in order to regulate the LV DC-link and the DC/AC converter controls the voltage in the ST-fed distribution grid. The advantage of the three-stage-topology lies in the possibility to offer MV and LV DC connection, for DC energy resources integrations (e.g. wind plants in MV and electric vehicles charging stations in LV), while the one of the two-stage topology is the maturity of industrial solutions. The DC connection feature allows to manage the LV grid without impacting on the MV grid operation. If the ST operates the LV grid phases in unbalanced way, the MV DC/AC converter still manages a balanced current injection in the MV grid. For this reason, based on the SPNF location, the ST can choose the configuration of the distribution grid within two different operating modes, that are the three-phase and two-phase operations, to ensure the continuity during fault conditions. If a SPNF occurs within the LV power distribution

and LV terminal distribution regions (point B in Fig. 1), the ST maintains three-phase operation, with the phases shifted of $120°$. Under this assumption, the faulty phase is disconnected by the protection breaker or fuse, without affecting the healthy-phases. If the fault occurs in the main feeder (point A in Fig. 1) the ST switches in two-phase mode, where the phase-shift of the healthy phases is varied to optimize grid operations. Since the phase-shift of the ST can be controlled flexibly, the ST is able to deal with the fault located in LV main distribution region, instead of causing an outage of downstream grid.

In order to study the performance of ST, it is assumed that SPNF occurs in phase c and the respective phase-shift is between phase a and b. Therefore, the voltage and current of the two healthy phases can be expressed as

$$\begin{cases} u_{\mathrm{a}} = U_{\mathrm{m}} cos\left(\omega t\right) \\ u_{\mathrm{b}} = U_{\mathrm{m}} cos\left(\omega t - \vartheta\right) \end{cases} \quad (1)$$

$$\begin{cases} i_{\mathrm{a}} = I_{\mathrm{am}} cos\left(\omega t - \theta_{\mathrm{a}}\right) \\ i_{\mathrm{b}} = I_{\mathrm{bm}} cos\left(\omega t - \vartheta - \theta_{\mathrm{b}}\right) \end{cases} \quad (2)$$

where subscript m represents the amplitude of voltage and current, subscripts a and b represent the variables of phase a and b, respectively, ω the angular frequency in rad/s, θ the power factor angle, and ϑ the phase-shift.

Based on (2), the neutral-line current can be calculated as

$$i_{\mathrm{n}} = I_{\mathrm{am}} cos\left(\omega t - \theta_{\mathrm{a}}\right) + I_{\mathrm{bm}} cos\left(\omega t - \vartheta - \theta_{\mathrm{b}}\right) \quad (3)$$

According to the p-q theory [14] [15], the instantaneous power for two-phase system is

$$\begin{bmatrix} p \\ q \end{bmatrix} = \begin{bmatrix} u_{\mathrm{a}} & u_{\mathrm{b}} \\ -u_{\mathrm{b}} & u_{\mathrm{a}} \end{bmatrix} \begin{bmatrix} i_{\mathrm{a}} \\ i_{\mathrm{b}} \end{bmatrix} \quad (4)$$

where p is the instantaneous real power and q is the instantaneous imaginary power. By substituting (1) and (2) into (4), the instantaneous real power can be written as,

$$p = \bar{p} + \tilde{p} \quad (5)$$

where

$$\bar{p} = \frac{U_{\mathrm{m}}}{2} \left(I_{\mathrm{am}} \cos \theta_{\mathrm{a}} + I_{\mathrm{bm}} cos\theta_{\mathrm{b}}\right)$$
$$\tilde{p} = \frac{U_{\mathrm{m}}}{2} \left(I_{\mathrm{am}} \cos \left(2\omega t - \theta_{\mathrm{a}}\right) + I_{\mathrm{bm}} \cos \left(2(\omega t - \vartheta) - \theta_{\mathrm{b}}\right)\right) \quad (6)$$

The first term on the right hand side of (5) represents the constant component of the real power, while the second term is the oscillatory component of the real power. Although having an average equal to zero in half fundamental period, this oscillatory term impacts on the DC-link voltage of the ST.

B. ST-based Single Phase Fault Management

During the management of a single-phase to ground fault, the ST has two goals: 1) ensure its own safety, avoiding large current inflow in the AC grid and DC link voltage oscillations that can lead to disruption of semiconductors
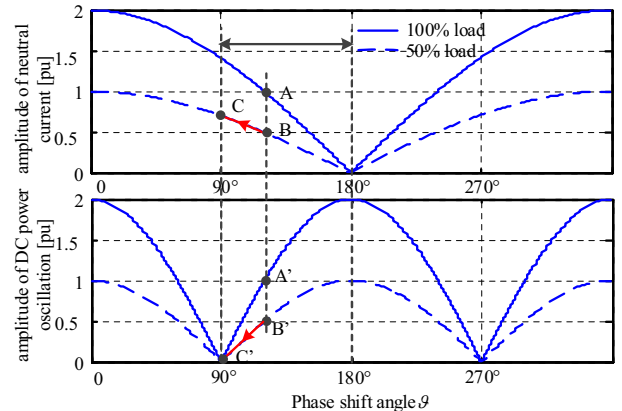

Fig. 3. Bi-phase operation concept.

and DC capacitors, respectively; 2) the safety of the ST-fed grid, guaranteeing acceptable power quality to the loads still connected and preserving the neutral line conductor from overload. As solution, the DC-link equivalent capacitance can be increased, adding more capacitors in parallel to the existing ones. However, this solution increases the costs, it decreases the system reliability, and it needs for additional space, that is not always available in urban sub-stations. Customized PWM strategies have been proposed to cope with the connection of 4-leg converters [16] or Neutral Point Clamped (NPC) converters [17] with neutral conductor to unbalanced distribution grid. In [17], new modulation strategies have been proposed for 4-leg and NPC converters, to balance the DC-link voltage in presence of large current unbalanced, showing that low DC voltage ripple can be achieved in case of asymmetrical voltage conditions. However, these papers deal with the connection of shunt elements, with the focus on obtaining balanced injection of power in case of asymmetric voltage. This voltage asymmetry is relatively small (few percent), and thus also the DC power oscillation results to be relatively small, too. In the ST case, the nominal grid power is processed (e.g., $1\,\mathrm{MVA}$), and thus the disconnection of one phase can lead to an oscillatory power up to $\pm333\,\mathrm{kVA}$. This power cannot be fully compensated with only modulation strategies. Steps forward were performed already in [18], where a new modulation strategy is proposed to reduce the DC-link power oscillation in case of unbalanced current. It shows that, in case of 40% higher current in one phase, the oscillation can be decreased from 21% with normal modulation to 9.5% with the proposed strategy. However, in the case of a disconnected phase, the power difference between the phases would be too large to be compensated just with modulation strategies.

To recognize a fault in the grid, methods such as Dynamic State Estimation-Based Protections (also known as setting-less protection) can be employed [19], [20]. This method is based on the confidence level of the system's measurements satisfying its dynamic model (i.e. its differential and algebraic equations), evaluated by means of dynamic state estimation. Observing the confidence level of not only the overall model but of individual sub-models facilitates the reliable separation between main bus bar faults (point A) and lower branch faults

(point B), as shown in Fig. 1.

The SPFM algorithm proposed in this work aims to minimize the 2nd harmonic power oscillation and at the same time to limit the neutral line current. The SPFM acts on the phase-shift between the two remaining healthy phases, shifting the phase angles in order to respect the DC-link voltage oscillation and neutral current limitations. Fig. 3 shows the amplitude of neutral line current and the DC power oscillations for full and partial load of the ST over the phase-shift ϑ. To be noted that the signs are discordant: as can be seen in Fig. 3, in the allowable range of $[90°\div180°]$, incrementing the angle, the DC voltage oscillation increases, while the neutral current amplitude decreases.
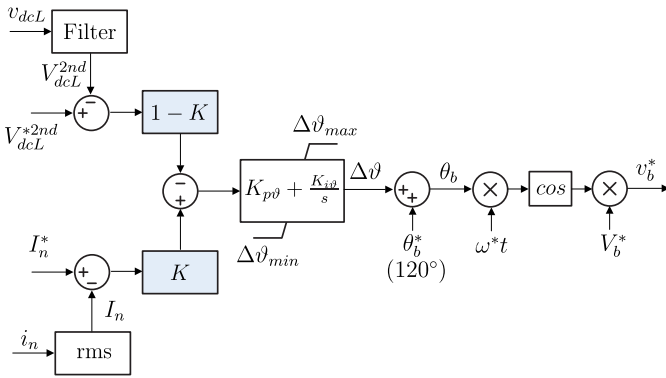

Fig. 4. SPFM control implementation.

The control scheme of the SPFM controller is described in Fig. 4. The controller tries to keep the DC voltage 2nd-order oscillation amplitude, within an acceptable limit (e.g., $\pm5\%$), and to restrain the neutral current amplitude flowing in the neutral conductor. A PI controller receives two error contributions from the DC-link voltage and the neutral current amplitude. Being the two objective function of different nature, a weight "K" has been introduced, in order to shift the contribution to the PI controller depending on the grid conditions (e.g., small neutral conductor or small DC-link capacitor). The PI regulates the phase-shift between the two remaining healthy phases, within the imposed limits. In first assumption, the limits $\Delta\vartheta_{min}$ and $\Delta\vartheta_{max}$ are set to $90°$ and $180°$, respectively. The SPFM algorithm is summarized in Fig. 5.

C. Capacitor lifetime analysis

As mentioned in the introduction, the DC-link capacitor is affected when a phase is lost. Besides the operating voltage, ambient temperature and ambient humidity, the thermal stress caused by the capacitor ripple current is considered as one of the main stressing factor of DC link capacitors. The hotspot temperature of the capacitor depends on the dissipated power and series equivalent resistance (ESR). The ESR is increasing for lower frequencies [21]. The oscillatory component of the real power is reflected as $100\,\text{Hz}$ ripple current in the DC link capacitor [22]. Hence, these low-order harmonic stress components, such as the 2nd harmonic, have a comparatively
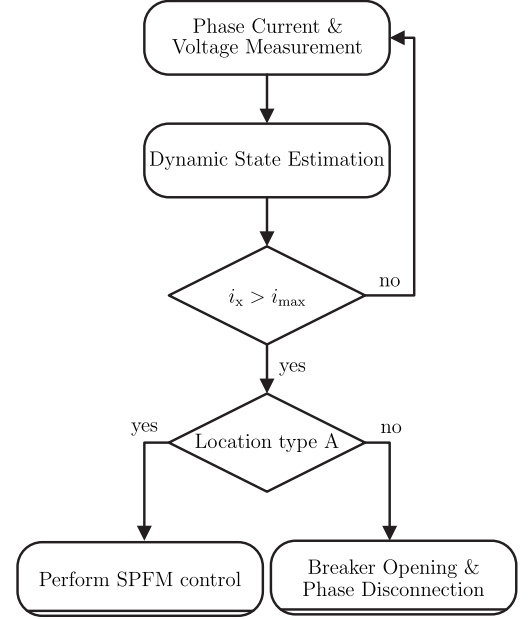

Fig. 5. SPFM control algorithm.

high impact on capacitor's dissipated power and consequently hotspot temperature and lifetime.

A general empirical capacitor lifetime model is given by (7), where L_0 is the lifetime under test conditions as given in the data sheet, V and V_0 are the operating and test voltage, respectively, n denotes a manufacturer dependent voltage stress constant, E_a is the activation energy, k_b stands for the Boltzmann constant and T_h and $T_{h,0}$ are the hotspot temperatures during operating and test conditions, respectively.

$$L = L_0 \left(\frac{V}{V_0}\right)^{-n} e^{\frac{E_a}{k_b}\left(\frac{T_{h0}-T_h}{T_{h0}T_h}\right)} \qquad (7)$$

Where the temperature dependency follows the Arrhenius law. Considering the activation energy of Aluminium-Electrolytic Capacitors (Al-Caps), $E_a = 0.94\,\text{eV}$, a common approximation [23], [24] of the Arrhenius law, which constitutes a doubling in lifetime for each $10\,\text{K}$ temperature decrease, yields:

$$L = L_0 \left(\frac{V}{V_0}\right)^{-n} 2^{\frac{T_{h,0}-T_h}{10\text{K}}} = L_0 H_V H_T \qquad (8)$$

The impacts of operating voltage and hotspot temperature can be represented with lifetime factors H_V and H_T, respectively. It can be observed that the lifetime is decreasing with increasing voltage and hotspot temperature. The hotspot temperature can be split into two parts, the ambient temperature and temperature variation depending on the operation conditions.

$$T_h = T_a + \Delta T_h \qquad (9)$$

As stated in [23], the temperature lifetime factor H_T can be split into two parts. Since the temperature appears in the

exponent of the exponential function, the lifetime factors are multiplied:

$$H_{\mathrm{T}} = 2^{\frac{T_{\mathrm{h},0} - T_{\mathrm{h}}}{10\mathrm{K}}} = 2^{\frac{T_{\mathrm{h},0} - T_{\mathrm{a}}}{10\mathrm{K}}} 2^{\frac{-\Delta T_{\mathrm{h}}}{10\mathrm{K}}} = H_{\mathrm{Ta}} H_{\mathrm{I}} \qquad (10)$$

The first part H_{Ta} characterizes the impact of ambient temperature, whereas the second part quantifies the capacitor ripple current impact on hotspot temperature increase. This term is denoted by ripple current factor H_{I}, and does not depend on ambient temperature.

In order to compare the changes in lifetime due to the control strategies it is assumed that the average operating voltage as well as the ambient temperature remain constant for all cases. Hence, the lifetime is only influenced by the capacitor ripple current and the lifetime change can be expressed by means of relative lifetime.

$$L_{\mathrm{rel,x}} = \frac{H_I}{H_{base}} \qquad (11)$$

where H_I and H_{base} are the capacitor ripple current factor with and without power 2nd harmonic oscillation. As it will be shown in the results section, a Fault Management approach must be implemented in the ST, in order to limit the impact of the second order power harmonic on the capacitor lifetime.

III. SIMULATION RESULTS

This section aims to verify what has been described analytically by means of PSCAD simulations of 18-bus Cigré benchmark LV distribution system (Fig. 6). In order to have a general view on the approach's effectiveness and its impact on the distribution grid, an heterogeneous typology of loads has been chosen. It has been considered the presence of aggregated single-phase loads $[L_1, L_2, L_4, L_5]$, a phase-to-phase load L_3 connected to phase b and c, an constant-torque controlled asynchronous machine A_{m1}, and a constant-power rectified load L_6. Furthermore, a photovoltaic (PV) plant and a battery energy storage system (BESS) have been installed in Bus 18 and Bus 10, and they are injecting $10\,\mathrm{kW}$ and $25\,\mathrm{kW}$, respectively. In Table I, the active and reactive powers of each load are listed.

TABLE I
ST-FED GRID DATA

Load	Variable	Phase A	Phase B	Phase C
L_1	Active Power (kW)	15.0	16.0	25.0
	Reactive Power (kVAr)	6.0	8.0	12.0
L_2	Active Power (kW)	25.0	20.0	25.0
	Reactive Power (kVAr)	10.0	12.0	15.0
L_3	Active Power (kW)	0.0	6.0	6.0
	Reactive Power (kVAr)	0.0	4.0	4.0
L_4	Active Power (kW)	6.0	0.0	0.0
	Reactive Power (kVAr)	2.0	0.0	0.0
L_5	Active Power (kW)	10.0	25.0	10.0
	Reactive Power (kVAr)	3.0	15.0	8.0
L_6	Active Power (kW)	10.0	/	/
	Capacitance (mF)	1.0	/	/
A_{m1}	Apparent Power (kVA)	4.0	4.0	4.0
	Power Factor (pu)	0.8	0.8	0.8

A single-phase to neutral fault with an impedance of $0.1\,\Omega$ occurs at 0 seconds in phase a at Bus 4. The ST, reading
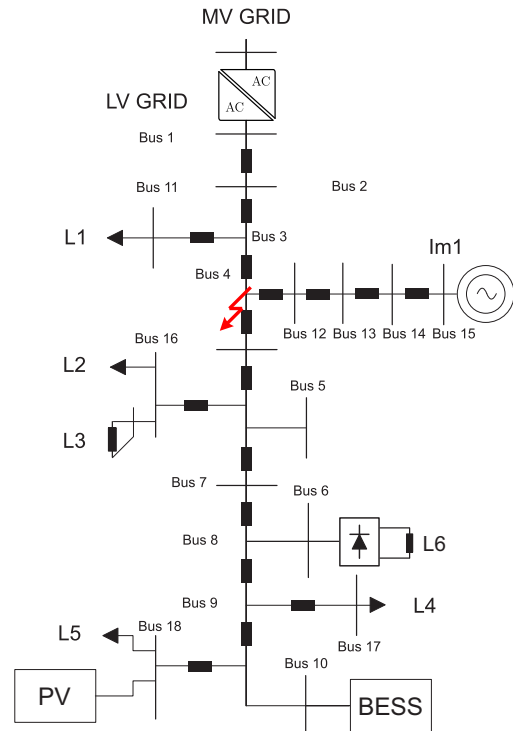

Fig. 6. 18-bus Cigré benchmark LV distribution system, taken from [25].

TABLE II
SMART TRANSFORMER DATA

ST parameter	Value	Grid Parameter	Value
S_{ST}	200 kVA	V_{rms}	230 V
C_{dcL}	5 mF	V_{dcL}	800 V
L_{LV}	0.1 mH	$I_{n,max}$	300 A

the short-circuit current (Fig. 7), blocks the phase a IGBTs, decreasing instantaneously the voltage, as shown in Fig. 8. It has been assumed that the ST is able to manage such current for a very short amount of time (i.e., half cycle). The system continues to work with a $120°$ shift between phase b and c. The connected resources (PV and BESS) remain connected for $200\,\mathrm{ms}$ following the fault, as recommended in [26], and they finally disconnect due to the low voltage protection. The induction machine remains connected for further $100\,\mathrm{ms}$, and then disconnects from the grid due to the high torque ripple.

The ST continues to operate in nominal condition ($120°$ phase angle shift) for around 1 second, until it activates the SPFM controller. This control action delay $d=1\,\mathrm{s}$ has been introduced to ensure the tripping of the connected three-phase loads and generators. As a first case, a gain $K = 0$ has been assumed, meaning that only the DC-link voltage controller contribution is considered. The SPFM controller aims to reduce the voltage oscillation to $5\,\%$ of the total voltage, that means to constrain it to $\pm 40\,\mathrm{V}$. Following the scheme in Fig. 3, the SPFM controller reduces the phase angle shift between phase b and c from $120°$ to $98°$ (Fig. 9), decreasing the voltage oscillation amplitude from $80\,\mathrm{V}$ to $40\,\mathrm{V}$, as shown in Fig. 10.

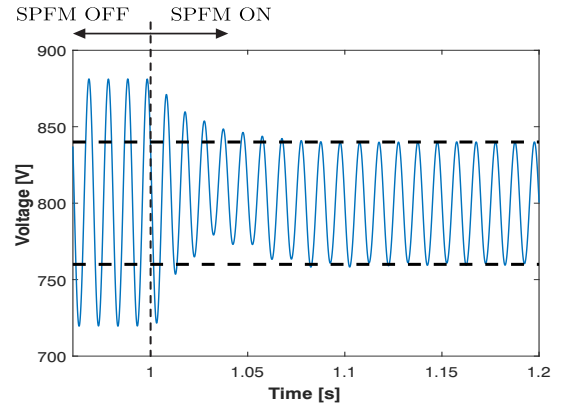One of the main advantages of the bi-phase operation is to
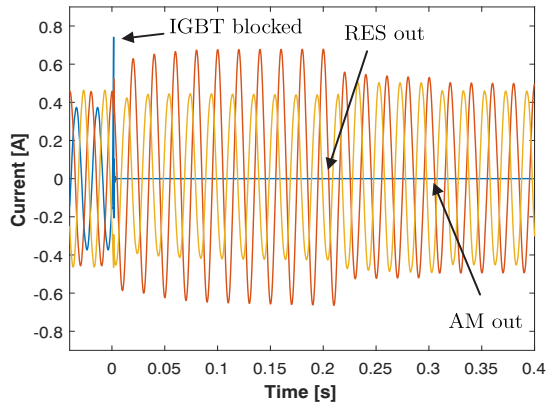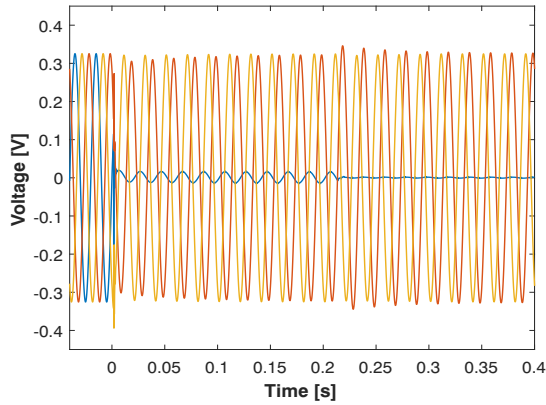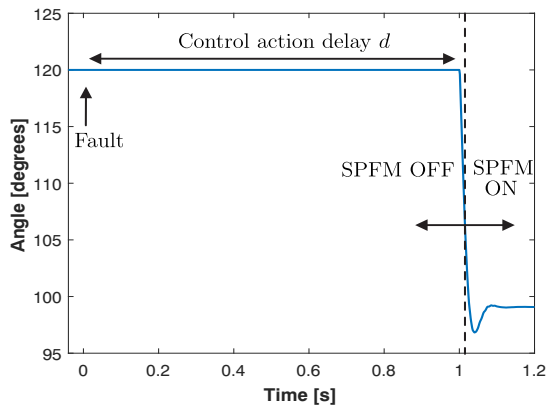
Fig. 7. ST line currents.

Fig. 8. ST phase-to-neutral voltages.

Fig. 9. ST Phase c angle.

maintain energy provision in the two healthy phases. Since the power consumption of residential electrical appliances is limited, their connection is usually single-phase. If the power consumption is analyzed before and after the fault, it can be noticed that large part of the load is still connected. As shown in Fig. 11, the power consumption of the grid before the fault is about 185 kW, considering 30 kW of power injection from PV and BESS. After the fault, the power consumption drops in average to 140 kW, meaning that in this test case almost 65 % of the load is still supplied. Providing still energy to the remaining two healthy phases represents a clear advantage in

Fig. 10. ST DC-link voltage.

terms of quality of the service that the ST has with respect to the conventional power transformer.
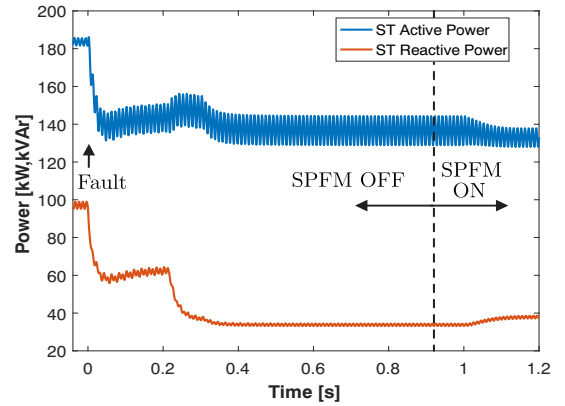

Fig. 11. ST-fed grid active (blue) and reactive (red) power consumption.

However, the application of the SPFM can affect the neutral conductor, violating its ampacity. The phase shift impacts also on the neutral current amplitude, that passes from about 250 A to 346 A, overloading the neutral conductor. Indeed, for a 200 kW ST, 300 A cables are considered both for the phases and for the neutral conductor. Thus, as shown in the following sections, the neutral conductor ampacity violation must be taken into account in calculating the angle shift.
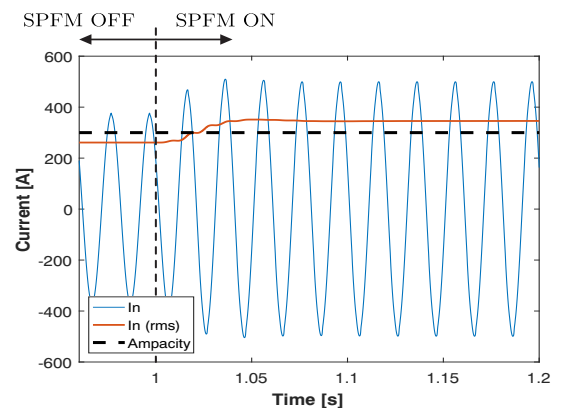

Fig. 12. Neutral current flowing in the ST bus.

IV. Discussion on bi-phase operations on the ST-fed grid loads

The LV grid is characterized by single-phase loads, corresponding to household and small commercial electrical appliances. In case of disconnection of one phase and consequent phase shift of the healthy phases, these loads do not notice any difference, considering also the smooth transition between the three- and two-phase systems. However, this consideration does not apply for three-phase and phase-to-phase loads. For the first category, missing one phase leads to a disconnection of the load. Unless any intelligent algorithm is implemented in the loads, that recognize the two-phase system and adapts the load power consumption to it. That can be the case of rectified constant power loads, where the loss of a phase corresponds to a decrease of the DC-link voltage and large instantaneous power oscillations, but leaving the active power basically unchanged. As can be noted from Fig. 13, both in the $120°$ and $98°$ phase shift case, the active power consumption remains substantially the same of the balanced case before fault, plus the increased losses caused by lower DC-link voltage.
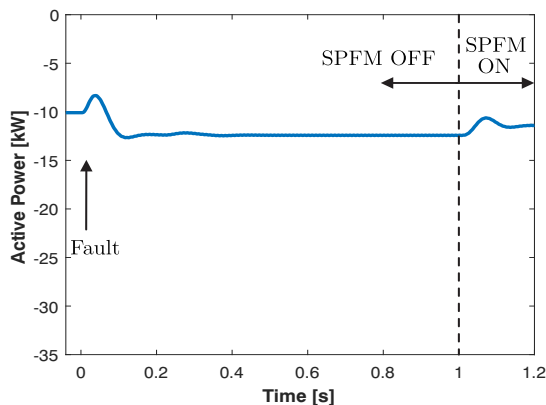

Fig. 13. Active power consumption of Load L_6 (three-phase constant power rectified load).

In some countries, like US, some loads are connected to the distribution grid with a phase-to-phase connection (e.g., delta-connection) [27], in order to increase the operating voltage and to limit the losses. In case of switching to the two-phase system, upper and lower voltage violations for these loads can be found in certain conditions. As can be noted in Fig. 14, if the SPFM shifts the angle to $180°$ to reduce the neutral current, the resulting voltage seen by the load is two times the phase-to-ground voltage, corresponding to 1.15 pu of the phase-to-phase voltage (Fig. 14). On the other hand, if the angle is shifted to $90°$, the resulting phase-to-phase voltage is equal to about 0.8 pu. For this reason, if phase-to-phase loads are present in the distribution grid, the permitted phase angle shift range has to be limited as depicted by the red area in Fig. 14.

As observed in the zoom of Fig. 14, to respect the limit of $\pm 10\%$ voltage variation from the nominal value, the phase angle shift in these phases has to be constrained to the range $\theta \in [102.4°, 144.6°]$. This constraint leads to find a suboptimal solution to the minimization of the power oscillation or neutral current, but it allows the connection of phase-to-phase loads within the safety limits.
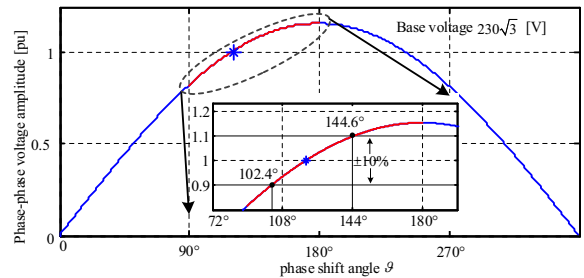

Fig. 14. Phase shift allowable range (red line) in case of phase-to-phase loads connected to the healthy phases.

In the case of minimization of the voltage ripple, when the SPFM controller decides to apply the new angle shift ($98°$), the phase $b-c$ voltage drops from 0.96 pu to 0.85 pu, violating the voltage lower limit of 0.90 pu, as can be observed in Fig. 15.
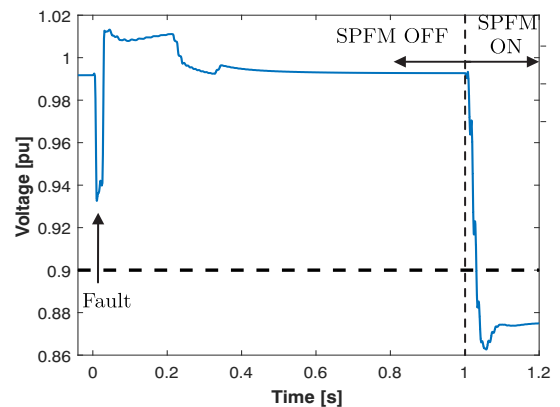

Fig. 15. Phase-to-phase load L_3 phase $b - c$ voltage.

V. Multi-objective SPFM algorithm

As demonstrated in the previous two sections, the SPFM algorithm has to respect several constraints (neutral current ampacity, phase-to-phase voltage limit) when minimizing the DC-link voltage oscillation. Thus, to avoid a violation of the neutral conductor ampacity, a relaxing of the DC-link voltage oscillation amplitude constraints is needed. Moreover, the angle restrictions for phase-to-phase load connection must be applied. For these reasons, in the SPFM controller shown in Fig. 4, the weight factor K has been optimized with the "Optimal Run" toolbox of PSCAD in order to obtain a tradeoff between neutral current overload and DC-link voltage oscillation violation. The threshold to find the optimum has been set to 10^{-3}, and the "Golden Area" algorithm has been used. The goal is achieved after 14 iterations, where the optimal weight K results to be $K = 0.73$.

The effects of the new angle shift have been plotted in Fig. 16, red curve. As can be seen, the angle shift is increased from $98°$ to $106°$, which results to be within the allowed limits for phase-to-phase loads.

As results of the multi-objective optimization, the neutral conductor current is decreased to 323 A (Fig. 17, red curve) instead of the starting 346 A and the DC-link voltage oscillation are increased to 53 V, as depicted in Fig. 18, red curve. As
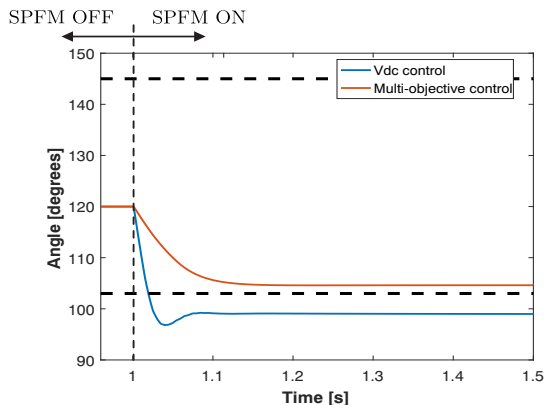
Fig. 16. ST Phase c angle in case of DC-link voltage minization control (blue line) and Optimal control considering neutral conductor ampacity and phase-to-phase voltage limits.
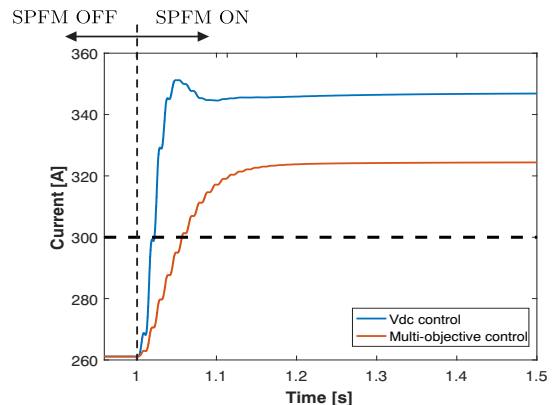

Fig. 17. Neutral current flowing in the ST bus in case of DC-link voltage minization control (blue line) and Optimal control considering neutral conductor ampacity and phase-to-phase voltage limits.
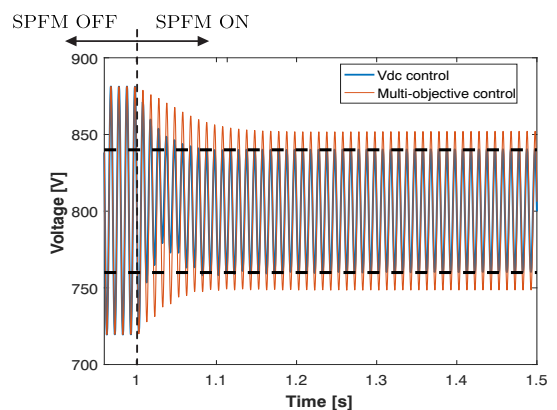

Fig. 18. ST DC-link voltage in case of DC-link voltage minization control (blue line) and Optimal control considering neutral conductor ampacity and phase-to-phase voltage limits.

Fig. 19. Phase-to-phase load L_3 phase $b - c$ voltage in case of DC-link voltage minization control (blue line) and Optimal control considering neutral conductor ampacity and phase-to-phase voltage limits.
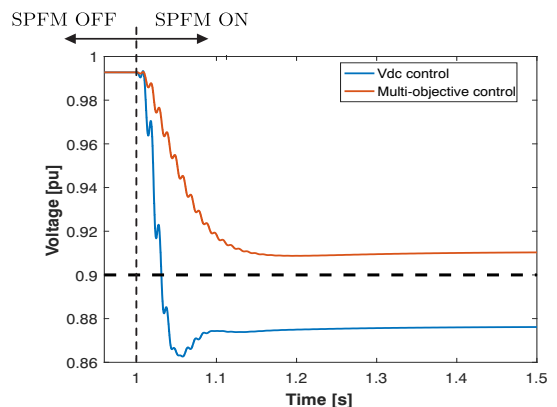
can be noted from the results, if the neutral current is taken into account in the optimization, a sub-optimal result is found for the DC-link capacitor. Thus, it is important to quantify the increased impact of the voltage oscillations on the capacitor lifetime

Due to the power dissipation at the ESR of the 100 Hz ripple current flowing through the capacitor, the capacitor hotspot temperature is increased. Following the analysis in section II-C, the lifetime of the capacitor is decreased with increasing hotspot temperature. Table III summarizes the relative lifetime for V_{dc} control and multi-objective SPFM algorithm with respect to the base case with SPFM turned off. It can be concluded that both SPFM concepts are beneficial for the DC-link capacitor's lifetime. With the V_{dc}, the relative lifetime of capacitor is increased of more than 5 times, while with the multi-objective control it is increased of 3.4 times.

TABLE III
RELATIVE CAPACITOR LIFETIME ANALYSIS

	SPFM OFF	V_{dc}	Multi-objective
Voltage oscillation [V]	80	40	53
Ripple current (rms) [A]	177.7	88.9	117.7
Temperature Rise [K]	31.6	7.9	13.9
Relative lifetime	1	5.2	3.4

Respecting the angle limits for phase-to-phase load connection, the load L_3 placed between phase b and c has a limited voltage drop (0.91 pu instead of 0.85 pu), as shown in Fig. 19, red curve, and the quality of the service has been respected ($\pm 10\,\%$ of the nominal voltage).

VI. EXPERIMENTAL VALIDATION

In order to further validate the theoretical analysis and simulation results, a microgrid setup with a 15 kW four-leg converter and three-phase passive load has been built in laboratory. The lab setup, as well as the control structure are shown in Fig. 20. Two Danfoss converters are connected in parallel to obtain the four-leg configuration. The ST-converter DC link is controlled by a programmable DC-source, and the ST hardware is controlled by a "dSPACE MicroLab Box"

control board. The corresponding hardware circuit parameters are summarized in Table IV.

At first, the two working conditions with phase shift $\theta_b = 180°$ and $\theta_b = 90°$ have been tested experimentally to confirm what has been described analytically in Section IIA. As can be seen in Fig. 21, with a phase shift of $\theta_b = 180°$, the neutral current is null, while the ST active power shows a
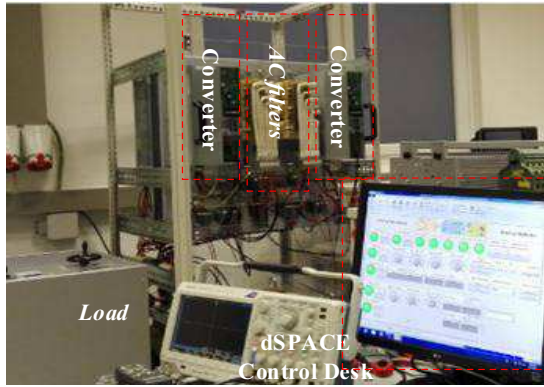
(*a*)
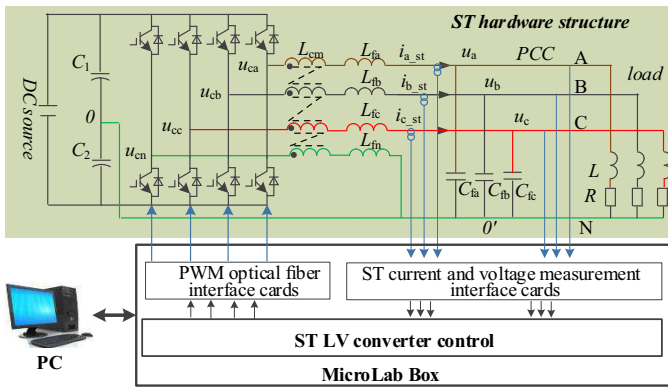
(*b*)

Fig. 20. Experimental setup: (*a*) converters used for 4-leg configuration and control board; (*b*), schematic of the setup.

Fig. 21. Test case $\theta_b = 180°$: ST active power (blue line on top), phase b and c voltages (cyan and purple line in the middle), neutral line current (green line on bottom).

Fig. 22. Test case $\theta_b = 90°$: ST active power (blue line on top), phase b and c voltages (cyan and purple line in the middle), neutral line current (green line on bottom).

TABLE IV
HARDWARE PARAMETERS OF THE EXPERIMENTAL SETUP

Parameters	Symbol	Value
Switching Frequency	f_s	10 kHz
Nominal Voltage	u	$100\,V_{pk-pk}$
Common mode filter inductance	L_{cm}	5.5 mH
Differential mode filter inductance	L_f	1.6 mH
Filter Capacitance	C_f	6 μF
Load Resistance	R	25Ω

$0.8\,kW_{pk-pk}$ oscillation, corresponding to $0.4\,kW$ DC and $\pm 0.4\,kW$ oscillatory components. If the phase shift reaches $\theta_b = 90°$ (Fig. 22), the opposite situation occurs: the ST active power is practically constant, but the neutral current shows a $5.65\,A_{pk-pk}$ oscillation.

However, the grid conditions may need for a tradeoff between power oscillation and neutral current. For this reason in Fig. 23, all the angles in the range $\theta \in [90°, 180°]$ are swiped dynamically to show the active power and neutral current behavior in different angle shift condition. As can be noted, at the beginning ($\theta_b = 90°$) and at the end ($\theta_b = 180°$) of the transient, the situations already shown in Fig. 22 and Fig. 21 occur, respectively. During the transient, an optimal area is identified $\theta \in [100°, 110°]$, where a tradeoff between the active power oscillation and neutral current amplitude can be found, depending on the DC capacitor and neutral

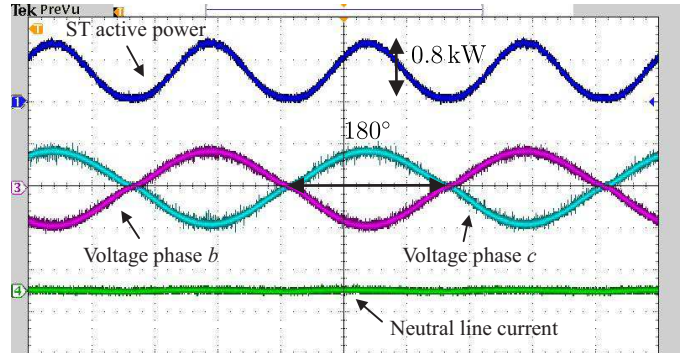conductor size. This confirms the choice of $\theta_b = 106°$ as optimal angle in Section V analysis.
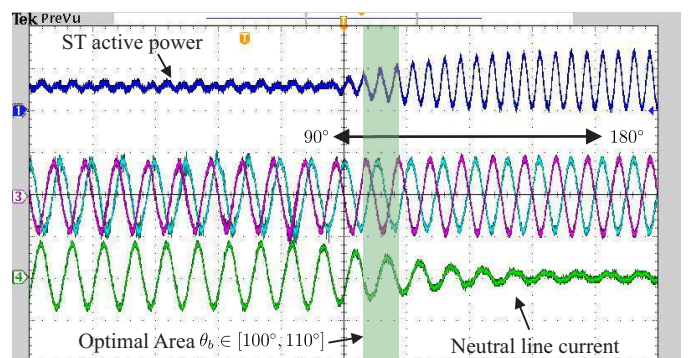
Fig. 23. Test case $\theta \in [90°, 180°]$: ST active power (blue line on top), phase b and c voltages (cyan and purple line in the middle), neutral line current (green line on bottom).
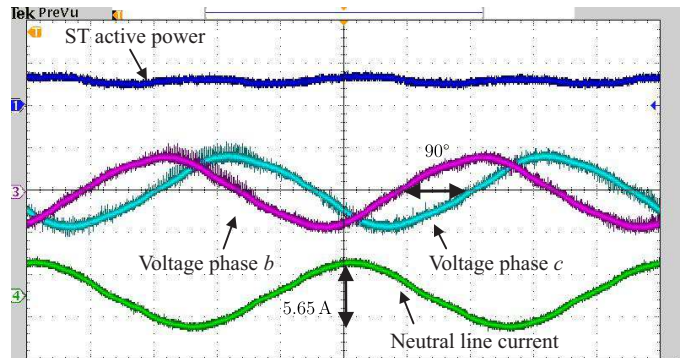
VII. CONCLUSIONS

In this paper, a Single Phase-to-Neutral fault management for Smart Transformers application has been proposed. The Smart Transformers, controlling the voltage waveform, is able to increase the controllability in the ST-fed grid. In case of a single-phase grid fault, the ST can rapidly block the faulty current and keep feeding the remaining two healthy-phases.

However, this heavy unbalance causes a high power 2nd harmonic oscillation and thus large voltage oscillation in the Smart Transformer LV DC-link. This leads to require a more frequency maintenance of the ST, in order to avoid unplanned outage due to failures of aged capacitor. The proposed Single-Phase Fault Management control in this paper explores the possibility to shift the angle between the two remaining phases in order to minimize the DC-link voltage oscillation, and, at the same time, preserving the neutral conductor from overload. The results show how the ST is able to reduce the DC-link oscillation of 33%, while decreasing the current overload in the neutral conductor. This control decreases the impact of the power 2nd oscillation on the DC-link, increasing the relative lifetime of the DC-link capacitor of 3.4 times with respect the case without fault management control, and thus the intervention time for maintenance squads of distributed system operators to repair the faulty section. Furthermore, the paper discusses on the impact on phase-to-phase and rectified loads, and shows that the SPFM control has limited impact on their normal operations and the grid codes are still fully respected.

REFERENCES

[1] G. Parise, L. Parise, L. Martirano, and A. Germole, "Service continuity safety by design: The relevance of electrical power-system architectures in hospitals," *IEEE Industry Applications Magazine*, vol. 22, no. 1, pp. 68–74, Jan 2016.

[2] I. Hernando-Gil, H. Shi, F. Li, S. Djokic, and M. Lehtonen, "Evaluation of fault levels and power supply network impedances in 230/400 v 50 hz generic distribution systems," *IEEE Transactions on Power Delivery*, vol. 32, no. 2, pp. 768–777, April 2017.

[3] M. Liserre, G. Buticchi, M. Andresen, G. De Carne, L. F. Costa, and Z. X. Zou, "The smart transformer: Impact on the electric grid and technology challenges," *IEEE Industrial Electronics Magazine*, vol. 10, no. 2, pp. 46–58, Summer 2016.

[4] G. De Carne, G. Buticchi, M. Liserre, and C. Vournas, "Load control using sensitivity identification by means of smart transformer," *IEEE Transactions on Smart Grid*, vol. 9, no. 4, pp. 2606–2615, July 2018.

[5] S. E. Networks. Lv engine. [Online]. Available: https://www.spenergynetworks.co.uk/pages/lv_engine.aspx

[6] G. De Carne, M. Liserre, and C. Vournas, "On-line load sensitivity identification in lv distribution grids," *IEEE Transactions on Power Systems*, vol. 32, no. 2, pp. 1570–1571, March 2017.

[7] A. Zidan, M. Khairalla, A. M. Abdrabou, T. Khalifa, K. Shaban, A. Abdrabou, R. E. Shatshat, and A. M. Gaouda, "Fault detection, isolation, and service restoration in distribution systems: State-of-the-art and future trends," *IEEE Transactions on Smart Grid*, vol. 8, no. 5, pp. 2170–2185, Sept 2017.

[8] P. S. Moses and M. A. S. Masoum, "Three-phase asymmetric transformer aging considering voltage-current harmonic interactions, unbalanced nonlinear loading, magnetic couplings, and hysteresis," *IEEE Transactions on Energy Conversion*, vol. 27, no. 2, pp. 318–327, June 2012.

[9] J. E. Huber and J. W. Kolar, "Optimum number of cascaded cells for high-power medium-voltage multilevel converters," in *2013 IEEE Energy Conversion Congress and Exposition*, Sept 2013, pp. 359–366.

[10] D. P. Stojanovic, L. M. Korunovic, and A. Jovic, "Measurement and analysis of neutral conductor current in low voltage distribution network," in *IEEE EUROCON 2009*, May 2009, pp. 1481–1486.

[11] J. C. Wu, H. L. Jou, H. H. Hsaio, and S. T. Xiao, "A new hybrid power conditioner for suppressing harmonics and neutral-line current in three-phase four-wire distribution power systems," *IEEE Transactions on Power Delivery*, vol. 29, no. 4, pp. 1525–1532, Aug 2014.

[12] B. Singh, P. Jayaprakash, T. R. Somayajulu, and D. P. Kothari, "Reduced rating vsc with a zig-zag transformer for current compensation in a three-phase four-wire distribution system," *IEEE Transactions on Power Delivery*, vol. 24, no. 1, pp. 249–259, Jan 2009.

[13] H. Ge and S. Asgarpoor, "Reliability and maintainability improvement of substations with aging infrastructure," *IEEE Transactions on Power Delivery*, vol. 27, no. 4, pp. 1868–1876, Oct 2012.

[14] J. L. Afonso, M. J. S. Freitas, and J. S. Martins, "p-q theory power components calculations," in *2003 IEEE International Symposium on Industrial Electronics (Cat. No.03TH8692)*, vol. 1, June 2003, pp. 385–390 vol. 1.

[15] T. Furuhashi, S. Okuma, and Y. Uchikawa, "A study on the theory of instantaneous reactive power," *IEEE Transactions on Industrial Electronics*, vol. 37, no. 1, pp. 86–90, Feb 1990.

[16] R. Zhang, V. H. Prasad, D. Boroyevich, and F. C. Lee, "Three-dimensional space vector modulation for four-leg voltage-source converters," *IEEE Transactions on Power Electronics*, vol. 17, no. 3, pp. 314–326, May 2002.

[17] M. Sharifzadeh, H. Vahedi, A. Sheikholeslami, P. Labb, and K. Al-Haddad, "Hybrid shmshe modulation technique for a four-leg npc inverter with dc capacitor self-voltage balancing," *IEEE Transactions on Industrial Electronics*, vol. 62, no. 8, pp. 4890–4899, Aug 2015.

[18] R. Zhu, G. Buticchi, and M. Liserre, "Investigation on common-mode voltage suppression in smart transformer-fed distributed hybrid grids," *IEEE Transactions on Power Electronics*, vol. 33, no. 10, pp. 8438–8448, Oct 2018.

[19] H. F. Albinali and A. P. S. Meliopoulos, "Resilient protection system through centralized substation protection," *IEEE Transactions on Power Delivery*, vol. 33, no. 3, pp. 1418–1427, June 2018.

[20] A. P. S. Meliopoulos, G. J. Cokkinides, P. Myrda, Y. Liu, R. Fan, L. Sun, R. Huang, and Z. Tan, "Dynamic state estimation-based protection: Status and promise," *IEEE Transactions on Power Delivery*, vol. 32, no. 1, pp. 320–330, Feb 2017.

[21] M. L. Gasperi, "Life prediction modeling of bus capacitors in ac variable frequency drives," in *Conference Record of 2005 Annual Pulp and Paper Industry Technical Conference, 2005.*, June 2005, pp. 141–146.

[22] H. Jedtberg, M. Langwasser, R. Zhu, G. Buticchi, T. Ebel, and M. Liserre, "Impacts of unbalanced grid voltages on lifetime of dc-link capacitors of back-to-back converters in wind turbines with doubly-fed induction generators," in *2017 IEEE Applied Power Electronics Conference and Exposition (APEC)*, March 2017, pp. 816–823.

[23] H. Jedtberg, M. Langwasser, R. Zhu, G. Buticchi, and M. Liserre, "Impacts of rotor current control targets on dc-link capacitor lifetime in dfig-based wind turbine during grid voltage unbalance," in *2017 IEEE Energy Conversion Congress and Exposition (ECCE)*, Oct 2017, pp. 3489–3495.

[24] S. G. Parler Jr and P. C. Dubilier, "Deriving life multipliers for electrolytic capacitors," *IEEE Power Electronics Society Newsletter*, vol. 16, no. 1, pp. 11–12, 2004.

[25] "Benchmark system for network integration of renewable and distributed energy resources c06.04.02," CIGRE, Tech. Rep., 2014.

[26] "Reference technical rules for the connection of active and passive users to the lv electrical utilities," CEI 0-21, Dec. 2012. [Online]. Available: http://www.ceiweb.it/doc/norme/12333.pdf

[27] K. Schneider, P. Phanivong, and J. Lacroix, "Ieee 342-node low voltage networked test system," in *2014 IEEE PES General Meeting — Conference Exposition*, July 2014, pp. 1–5.

Giovanni De Carne (S'14, M'17) received the bachelor and master degrees in Electrical Engineering from Bari Polytechnic (Italy) in 2011 and 2013, respectively. He got his PhD in 2018 at the Chair of Power Electronics at Kiel University, Germany with the thesis: Analysis of ST features for electric distribution grid within the ERC Grant project Highly Reliable And Efficient smart Transformer (HEART). He is currently working as a post-doctoral researcher in the Kopernikus Project "ENSURE", studying the ancillary services provision in AC grids by DC terminals. He has published more than 40 technical papers (more than 15 in international peer-reviewed journals).
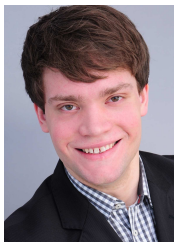
Marius Langwasser (S'16) received the B.Sc. and M.Sc. degrees in Electrical Engineering and Business Administration from Kiel University (Germany) in 2014 and 2016, respectively. Since 2016 he is working as a scientific staff member and PhD student at the Chair of Power Electronics at Kiel University, Germany. His research interests include control and protection of multi-terminal DC grids and ancillary service provision with HVDC.

Marco Liserre (S'00-M'02-SM'07-F'13) received the MSc and PhD degree in Electrical Engineering from the Bari Polytechnic, respectively in 1998 and 2002. He has been Associate Professor at Bari Polytechnic and Professor at Aalborg University (Denmark). He is currently Full Professor and he holds the Chair of Power Electronics at Kiel University (Germany). He has published over 300 technical papers (more than 100 of them in international peer-reviewed journals) and a book. These works have received more than 20000 citations. Marco Liserre is listed in ISI Thomson report The worlds most influential scientific minds. He is member of IAS, PELS, PES and IES. He has been serving all these societies in different capacities and he has received several IEEE awards.

Rongwu Zhu (S12-M15) received the B.Eng. in Electrical Engineering from Nanjing Normal University, Nanjing, China, in 2007 and Ph.D. degree in energy technology from Department of Energy Technology, Aalborg University, Aalborg, Denmark. From 2011-2012, he was a guest researcher with Aalborg University. He is currently a Postdoctoral Researcher with Chair of power electronics, at Christian-Albrechts-University of Kiel, Kiel, Germany. His research interests include high-power multilevel converters, nonlinear control, DC-grid and wind-farm power systems, smart-transformer-fed distribution generation system.